

Implications of the Quantum Noise Target for the Einstein Telescope Infrastructure Design

Philip Jones, Teng Zhang, Haixing Miao, and Andreas Freise
School of Physics and Astronomy, and Institute of Gravitational Wave Astronomy,
University of Birmingham, Edgbaston, Birmingham B15 2TT, United Kingdom
(Dated: April 6, 2024)

The design of a complex instrument such as Einstein Telescope (ET) is based on a target sensitivity derived from an elaborate case for scientific exploration. At the same time it incorporates many trade-off decisions to maximise the scientific value by balancing the performance of the various subsystems against the cost of the installation and operation. In this paper we discuss the impact of a long signal recycling cavity (SRC) on the quantum noise performance. We show the reduction in sensitivity due to a long SRC for an ET high-frequency interferometer, provide details on possible compensations schemes and suggest a reduction of the SRC length. We also recall details of the trade-off between the length and optical losses for filter cavities, and show the strict requirements for an ET low-frequency interferometer. Finally, we present an alternative filter cavity design for an ET low-frequency interferometer making use of a coupled cavity, and discuss the advantages of the design in this context.

I. INTRODUCTION

Current gravitational wave detectors, such as aLIGO [1] and Advanced Virgo [2], and plans for future detectors, such as Einstein Telescope (ET) [3–5], make use of a dual-recycled Michelson interferometer design with arm cavities, as shown in Figure 1. There are a few key additions over a simple Michelson interferometer, namely the power recycling mirror (PRM), the arm cavities, and the signal recycling mirror (SRM). The PRM acts to increase the effective input laser power;

the arm cavities increase the effective length of the arms; and the SRM reflects signal light back into the arms, providing a way to alter the bandwidth and peak sensitivity of the interferometer. Current detectors also make use of frequency-independent squeezing to increase quantum-noise limited sensitivity [6–8]. Future detectors will include frequency-dependent squeezing to improve quantum-noise limited sensitivity, which necessitates the addition of one or more filter cavities [9]. In addition, ET features a xylophone design, where two partially overlapping frequency ranges are investigated by different interferometer setups in the same location [10]. ET-HF operates in a tuned, broadband mode at high frequencies of $10\text{--}10^4$ Hz, and ET-LF in a detuned, narrow-band mode at low frequencies of $1\text{--}250$ Hz.

A fundamental property of interferometers is the trade-off between bandwidth and peak sensitivity, known as the Mizuno Limit [11]. The finite bandwidth of the arm cavities arises due to the gravitational wave signal light gaining extra phase with increasing frequency (phase dispersion), and eventually no longer resonating. This is a property of all cavities, including the signal recycling cavity (SRC). Up until now, the length of the SRC has been largely ignored, as it is often negligible compared to the length of the arms (~ 55 m in aLIGO, compared to 4 km arm cavities). This allowed us to treat the response of the SRC as practically instantaneous relative to the arms, and thus the whole ITM-SRM system can be thought of as a single compound mirror. For future detectors, especially ET, this may no longer be the case; the initial proposed SRC length is 300 m [5]. We therefore need to understand the consequences of a non-negligible SRC length on detector design.

Another variable worth investigating is the length of the filter cavities in ET. Whereas the ET design study assumed 10 km long filter cavities, in more recent discussions a reduction of this length to 1 km for ET-LF and 300 m for ET-HF is being considered. As the performance of filter cavities is determined solely by their loss

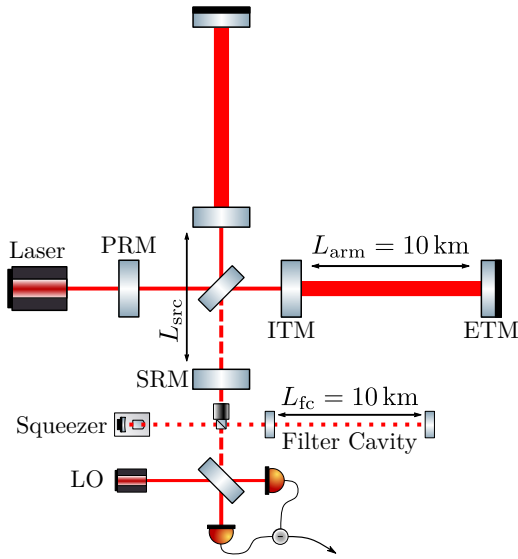


FIG. 1. Simplified interferometer design considered in this paper, with parameters shown for ET-HF. The signal recycling cavity length L_{src} is the total distance between the signal recycling mirror (SRM) and the input test mass (ITM). The squeezer is a frequency-independent squeezed vacuum source. ET makes use of a balanced homodyne detection scheme, comprised of two photodiodes and a local oscillator (LO). For ET-LF the only addition is an extra filter cavity.

per unit length [9, 12], it is necessary to understand how this reduction in length would affect the quantum-noise limited sensitivity of ET.

II. SIGNAL RECYCLING CAVITY LENGTH

There are a few motivating factors for an increased SRC length in ET compared to that of current detectors. In the arm cavities, a relatively large beam radius is required in order to reduce coating thermal noise [13]. This is especially important for ET-HF, which is almost entirely limited by coating thermal noise around 40–200 Hz. At the central beamsplitter, however, a small beam radius is desirable; it would allow smaller optics and better control of scattered light in the central interferometer. In order to achieve such a change in the beam sizes, a lens or telescope must be placed between the ITMs and the beamsplitter. A short distance between the ITMs and beamsplitter, and hence a short SRC, would require stronger focusing elements with more stringent optics requirements to avoid introducing aberrations and noise. Another factor leading to a long SRC is the use of cryogenic mirrors in ET-LF. To achieve sufficient cooling of the ITMs, cryoshields along the vacuum tubes are required to reduce the solid angle under which the cold ITMs are exposed to room temperature parts of the instrument. The lengths of the cryoshields (several tens of meters) also add to the SRC length.

Previous models used throughout the collaboration, and in the ET Design Study [5], assumed that the SRC length can be neglected. This is no longer valid. We therefore need to model and understand what effects SRC length has on the sensitivity of ET, and how to choose optimal SRC parameters for a given length. Figure 2 shows the effects of different SRC lengths on the quantum noise performance of the example ET-HF setup from Figure 1, compared to that given in the ET design (ET-D). All modelling throughout this paper was performed using the frequency-domain modelling software FINESSE [14, 15]. It should be noted that our investigations do not yet include the effects of higher-order modes and beam shapes. These effects should be studied further in the future, as changing the length of the SRC impacts the detector design in other ways as well, for example, with respect to avoiding higher-order mode resonances and parametric instabilities [16].

From Figure 2, we see that increasing the SRC length L_{src} leads mostly to a change in the gradient of the quantum noise performance at high frequencies, with a small increase in sensitivity at certain other frequencies. This arises due to a change in the coupled cavity dynamics of the interferometer, and to understand how to compensate for it, we must first understand exactly why this effect occurs.

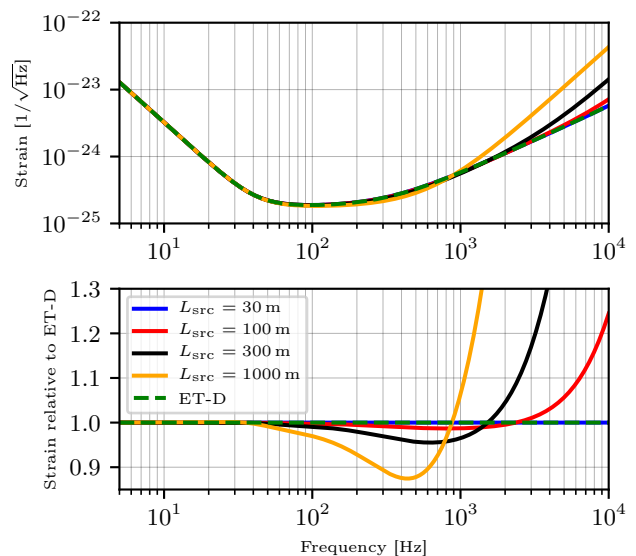


FIG. 2. Effect of increasing L_{src} on ET-HF, without changing other interferometer parameters. For the value $L_{\text{src}} = 300$ m proposed in the ET Design Study [5], quantum noise deviates from the design curve significantly above 2 kHz, reaching a factor of 2 increase at ~ 7.5 kHz.

A. The SRC-Arm System as a Coupled Cavity

For $L_{\text{src}} \ll L_{\text{arm}}$, where L_{arm} is the interferometer arm length, we can treat the SRM-ITM system as a kind of compound mirror, the only effect of which is to alter the output from the arm cavities. This is described in Buonanno & Chen [17], which for the tuned SRM case gives the half-bandwidth of the SRC-arm system as

$$\gamma_0 = \frac{1 + r_{\text{src}}}{1 - r_{\text{src}}} \gamma_{\text{arm}}, \quad (1)$$

where r_{src} is the amplitude reflectivity of the SRM, and $\gamma_{\text{arm}} = cT_{\text{itm}}/4L_{\text{arm}}$ is the half-bandwidth of the arm cavity, with T_{itm} the power transmissivity of the ITMs. When the SRC is comparable in length to the arm cavities, complicated coupled cavity effects come into play. We should therefore have a brief look at the basic properties of coupled cavities before proceeding.

The distinguishing feature of a coupled cavity is the presence of a split resonance. A single cavity exhibits an infinite number of equally spaced resonances, where the frequency difference between consecutive resonances is known as the free spectral range (FSR). A coupled cavity consists of two cavities, each with their own FSR, and will exhibit resonance peaks whenever a field is resonant in either of these cavities. For a field that is resonant in both cavities (i.e. every common multiple of both FSRs), a split resonance can occur, where two closely-spaced resonance peaks are observed instead of one. In the case where the two cavities have the same length, a derivation of the frequency difference between the two peaks is given by Thüring, Lück and Danzmann [18]. If we then

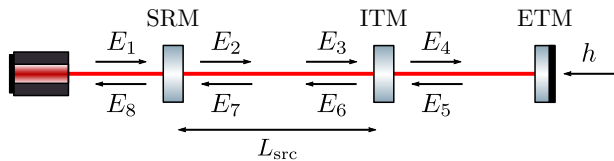


FIG. 3. Simplified ET coupled cavity setup. Each of the E_n are the full field at that point, including all frequencies. Here we are interested only in observing how the value of L_{src} affects the shape (not absolute value) of the strain-output transfer function of the interferometer, in a numerical simulation. In this model the only purpose of the laser is to provide power in the arm cavity, so it can be placed at either end of the setup.

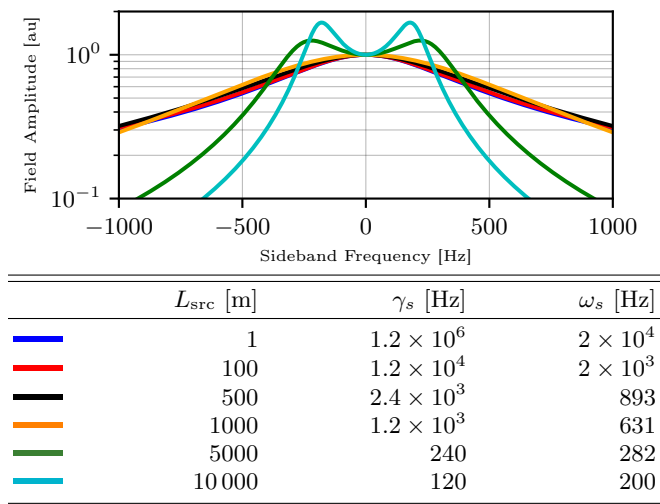


FIG. 4. Effect of SRC length on the strain-output transfer function for the simplified ET-HF setup shown in Figure 3, normalised to $L_{\text{src}} = 1$ m at 0 Hz. As L_{src} increases, ω_s grows in relation to γ_s until they are comparable in size and the split resonance becomes visible.

assume that $T_{\text{itm}} \ll 1$, Martynov *et al.* [19] provides formulas for the frequency difference between the two peaks ω_s , and the bandwidth of each peak γ_s :

$$\omega_s = \frac{c\sqrt{T_{\text{itm}}}}{2\sqrt{L_{\text{src}}L_{\text{arm}}}}, \quad \gamma_s = \frac{cT_{\text{src}}}{4L_{\text{src}}}, \quad (2)$$

where T_{src} is the power transmissivity of the SRM.

For sample ET-HF parameters of $T_{\text{src}} = 0.1$, $T_{\text{itm}} = 0.007$, $L_{\text{src}} = 100$ m & $L_{\text{arm}} = 10$ km, we obtain $\gamma_s = 12$ kHz, $\omega_s = 2$ kHz. As the bandwidth of the peaks is much greater than the separation, they are indistinguishable, and the whole system has a single resonance peak per FSR. However, as L_{src} increases, γ_s decreases faster than ω_s , and the two peaks become more resolved. For the simplified setup in Figure 3, the effects of increasing L_{src} are shown in Figure 4.

It should be noted that Equations (1) and (2) are only correct in their relevant extremes. In reality, interferometers operate somewhere between the two, where although

calculating the response of the setup in Figure 3 is simple, there is no analytical solution for the bandwidth of the one or two peaks present. However, Equations (1) and (2) are useful as a starting point for investigating the behaviour of a long SRC with numerical simulations.

It should now be clear why we see a decrease in sensitivity at high frequency for longer SRC lengths in Figure 2, as increasing L_{src} reduces the bandwidth of the coupled cavity resonance and decreases the magnitude of the frequency-splitting. To combat this, we can restore ω_s & γ_s to their original values, or as close as possible. For a change in SRC length from L_{src} to L'_{src} , we should therefore increase T_{src} & T_{itm} by the same ratio $L'_{\text{src}}/L_{\text{src}}$. By increasing T_{itm} , however, we change both the finesse of the arm cavities, and the gain of the power recycling cavity (PRC). This reduces the circulating arm power, and also redistributes power in the interferometer from the arm cavities to the PRC. If we then increase input power to restore the arm cavity circulating power, we can recover the original quantum noise sensitivity curve with a larger L_{src} , at the cost of increased power incident on the central beamsplitter and transmitted through the ITMs. This is undesirable as absorbed laser power causes thermal distortion of the optics, creating a thermal lens which can lead to mode mismatches and losses. Compensation for different values of L_{src} , along with power incident on the beamsplitter, is shown in Figure 5. A good compromise for ET-HF, including the beam expansion telescope, can be achieved with L_{src} of around 100 m. Figure 6 shows how the quantum noise at high frequencies scales with power incident on the central beamsplitter for this length.

So far we have only discussed the effect of increasing L_{src} on ET-HF. This is because, for any practical value of $L_{\text{src}} \lesssim 1$ km, the effect on the frequency range of interest for ET-LF (up to ≈ 30 Hz) is negligible; this is shown explicitly in Figure 7. Figure 4 provides the explanation for this behaviour. For a 1 km SRC, we have $\gamma_s = 1.2$ kHz, $\omega_s = 631$ Hz—the split resonances are still too wide to be individually resolved, and the splitting frequency is much greater than the top end of the frequency range of interest.

III. OPTIMISED FILTER CAVITIES FOR ET

In order to produce frequency-dependent squeezing to improve the quantum-noise limited sensitivity of ET, frequency-independent squeezed light is reflected from one or more filter cavities. This induces a frequency-dependent phase shift in the reflected light. The ET Design Study [5] considered 10 km long filter cavities. Shorter filter cavities are under consideration as a cost saving change to the design, as the vacuum and tunnel infrastructure are one of the main costs of the future observatory. Significantly shortened filter cavities would allow a simplification of the infrastructure design—example lengths being considered are a reduction from 10 km

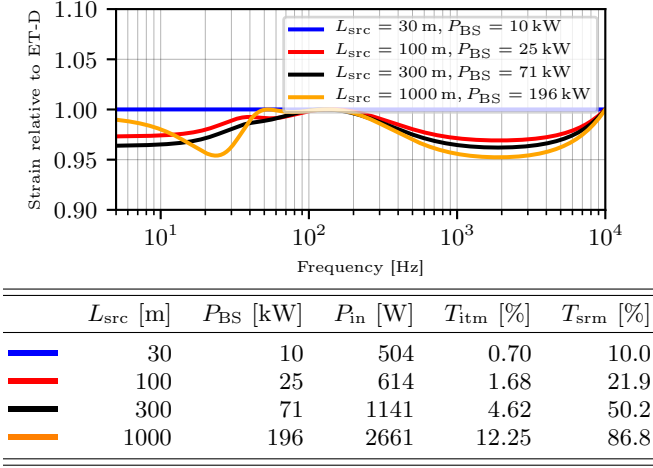


FIG. 5. Options for correcting for an increased SRC length in ET-HF. Parameters were found by numerically optimising to give the minimum beamsplitter power possible, without decreasing sensitivity relative to ET-D. Compared to the uncorrected curves in Figure 2, we no longer see a decrease in sensitivity at high frequency with increasing L_{src} , at the cost of increased power on the central beamsplitter—the minimum power required to keep below the original curve scales slightly less than linearly with SRC length. It is noteworthy that SRM transmissivity places a physical limit on how much γ_s can be increased for a given value of L_{src} . For $L_{\text{src}} > 1000$ m, this would start to constrain the design more strictly. It is also notable that the scaling relations from Equation (2) do not hold over the whole range of lengths shown; for $L_{\text{src}} = 1000$ m, the required mirror transmissivities are much lower than one would expect.

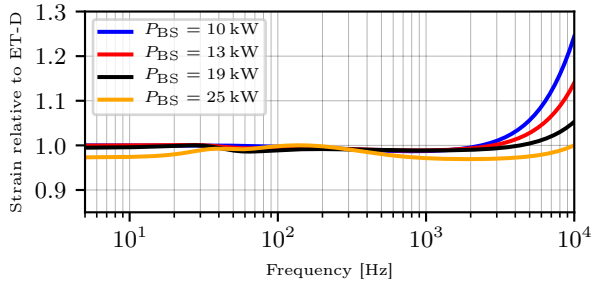


FIG. 6. Scaling of quantum-noise limited sensitivity with power incident on the central beamsplitter for a fixed SRC length of 100 m in ET-HF. For future high-power detector designs with significant SRC lengths, we can consider the trade-off between slightly reduced sensitivity due to quantum noise at high frequency, and increased noise due to thermal effects when compensating for SRC length.

down to 1 km for ET-LF, and 300 m for ET-HF. The performance of filter cavities is determined by their loss per unit length [9], and this reduction in length will lead to a corresponding increase in squeezing loss in the filter cavities. In practice, the optical loss will be determined by the detailed properties of the optical surface and the beam radius [20], the minimum value of which is dependent on cavity length. A simple extrapolation from

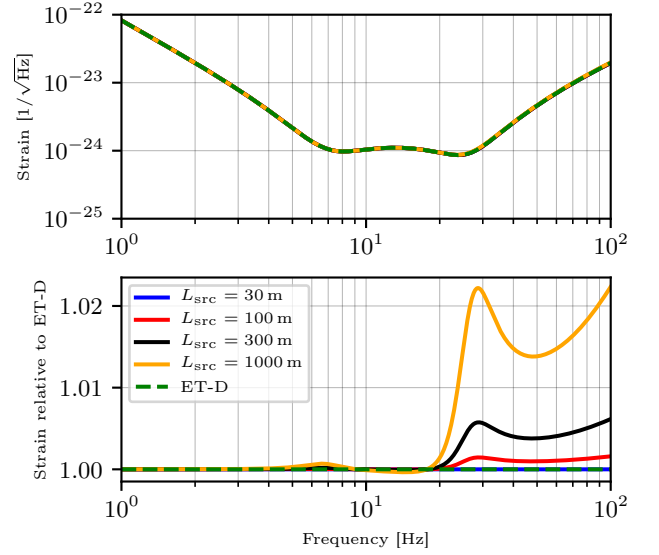


FIG. 7. Effect of increasing L_{src} on ET-LF, without changing any other interferometer parameters. We see that even for $L_{\text{src}} = 1$ km, the reduction in sensitivity is only 2 % at 30 Hz, and for a realistic length of 100 m, the effect is on the order of 0.1 %.

other experiments would suggest the following optical losses are achievable with current technology and techniques for the different filter cavity lengths [12]: 30 ppm @ 300 m, 40 ppm @ 1 km and 75 ppm @ 10 km. Throughout this section, we do not attempt to predict detailed optical losses, but provide quantum-noise limited sensitivity curves for a range of possible round-trip filter cavity power losses.

A. ET-HF

For ET-HF in its tuned, broadband configuration, only one filter cavity is required. In this case, an analytical solution for the optimal filter cavity detuning and bandwidth is given in [21, Equations (31, 33, 49, 50 & 53)] as

$$\Delta\omega_{\text{fc}} = \sqrt{1 - \epsilon}\gamma_{\text{fc}}, \quad (3)$$

$$\gamma_{\text{fc}} = \sqrt{\frac{2}{(2 - \epsilon)\sqrt{1 - \epsilon}}} \frac{\Omega_{\text{SQL}}}{2}, \quad (4)$$

$$\text{where } \epsilon = \frac{4}{2 + \sqrt{2 + 2\sqrt{1 + \left(\frac{2\Omega_{\text{SQL}}}{f_{\text{FSR}}\Lambda_{\text{rt}}^2}\right)^4}}} \quad (5)$$

$$\text{and } \Omega_{\text{SQL}} \simeq \frac{t_{\text{srm}}}{1 + r_{\text{srm}}} \frac{8}{c} \sqrt{\frac{P_{\text{arm}}\omega_0}{mT_{\text{itm}}}}. \quad (6)$$

Here, f_{FSR} is the free spectral range of the filter cavity, Λ_{rt}^2 is the round-trip power loss in the filter cavity, t_{srm} & r_{srm} are the amplitude transmissivity and reflectivity of

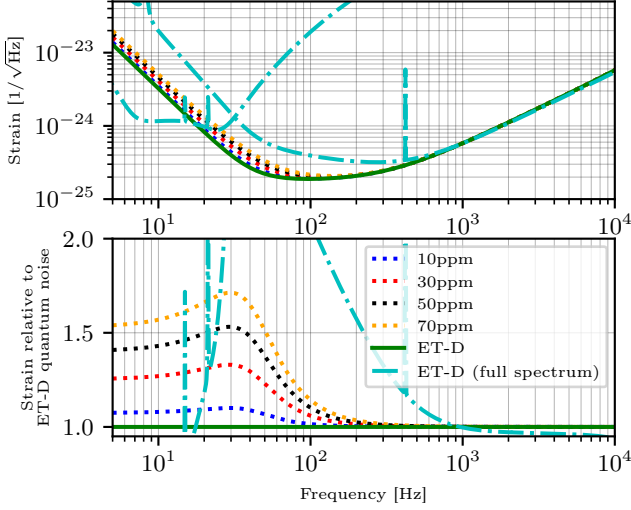


FIG. 8. The effect of filter cavity loss on ET-HF, with $L_{fc} = 300$ m. For a round-trip loss of 70 ppm, we see an increase in quantum noise of $\simeq 75\%$ at 30 Hz, relative to that of ET-D. However, ET-D is limited by thermal noise around this frequency, so the overall sensitivity is not affected. As filter cavity performance is determined by loss per unit length, the lower loss curves can be used to infer curves for other lengths e.g. a 700 m filter cavity with 70 ppm round-trip loss would give the 30 ppm curve shown.

L_{fc} [m]	Tuning [Hz]	Half-bandwidth [Hz]
300	-29.9520	5.2305

TABLE I. Optimal filter cavity parameters for ET-HF, with 70 ppm round-trip filter cavity loss.

the signal recycling mirror, P_{arm} is the circulating power in the arm cavities, ω_0 is the carrier frequency, m is the mass of the test masses, and T_{itm} is the power transmissivity of the input test mass mirror.

Figure 8 shows the effect of loss on ET-HF, with filter cavity length $L_{fc} = 300$ m, and Table I gives the optimal filter cavity parameters according to Equations (3) and (4). The effect of the increased losses is a reduction in the quantum-noise limited sensitivity at low frequencies, especially around 30 Hz. However, in this frequency band the current ET-HF design is entirely limited by thermal noise, so the overall sensitivity is not affected. We expect that upgrades to the interferometers in the long-term infrastructure of ET will reduce this thermal noise. Space for a filter cavity of modest length should therefore already be allocated in the initial infrastructure.

B. ET-LF

ET-LF operates with a detuned SRM, and thus requires two filter cavities to achieve optimal squeezing. Unlike in the single filter cavity case, no analytical so-

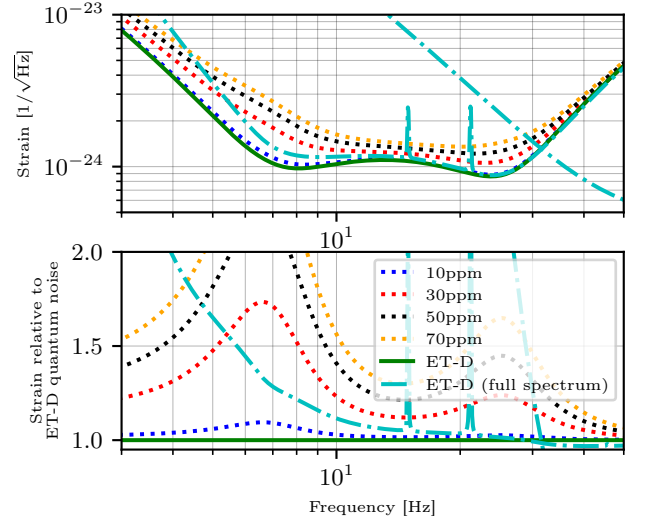


FIG. 9. The effect of filter cavity loss on ET-LF, with $L_{fc} = 1$ km. For a round-trip loss of 70 ppm, we see an increase in quantum noise of up to 160 % at 7 Hz, relative to that of ET-D (75 ppm loss, $L_{fc} = 10$ km), and a minimum of 30 % over the full spectrum below 30 Hz.

Filter	Tuning [Hz]	Half-bandwidth [Hz]
FC ₁	25.3574	5.6830
FC ₂	-6.6366	1.4468

TABLE II. Optimal filter cavity parameters for ET-LF, with 70 ppm round-trip filter cavity loss.

lution exists for multiple lossy filter cavities. A good approximation is provided by [22, Appendix A], however this assumes lossless filter cavities. Thus, we start with this approximation, and then optimise numerically. Figure 9 shows the effects of losses on ET-LF, with $L_{fc} = 1$ km, and Table II gives optimal filter cavity parameters. We see that a reduction in length leads to a much more stringent requirement for the optical loss to avoid spoiling the sensitivity at low frequencies around 7 Hz. The Virgo detector has already demonstrated round-trip losses of 55 ± 10 ppm in km-scale cavities [23]. These optical losses are dominated by deficiencies in the mirror surface quality, and research is ongoing to identify and mitigate the loss due to light scattering by surface defects. Using the same technology it should currently be possible to realise a 1 km long cavity with round-trip losses of less than 40 ppm. It is reasonable to believe that in the future we can improve the mirror surface quality further, to achieve a round trip loss of 20 ppm, with careful use of state-of-the-art technologies and care regarding polishing, coating, handling and installation.

The main motivation for reducing the filter cavity lengths in ET-LF is the cost of the infrastructure. There is a disincentive to use the main 10 km tunnels for the arm cavities as well as two filter cavities, due to the scal-

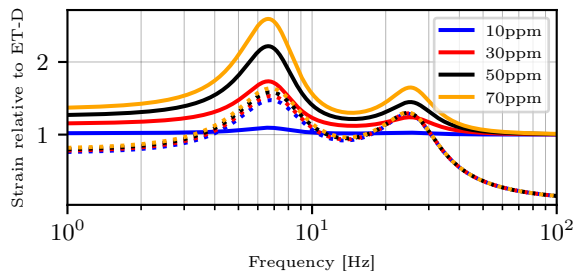


FIG. 10. Comparison of a detuned ET-LF with 2×1 km filter cavities (solid curves) and a tuned ET-LF with 1×10 km filter cavity (dotted curves). For a round-trip power loss > 30 ppm, the tuned system with one filter cavity performs better across the entire frequency range, especially at high frequencies.

ing of excavation cost with tunnel diameter. Given the lack of a low-frequency dip for a 1 km filter cavity with loss $\gtrsim 20$ ppm, it is interesting to compare the previous results to the performance of a tuned SRM for ET-LF with only one filter cavity. A comparison of this tuned ET-LF with a single 10 km long filter cavity, and a detuned ET-LF with two 1 km long filter cavities, is shown in Figure 10. For a round-trip power loss > 30 ppm, the tuned system with one filter cavity performs better than the detuned system with two short filter cavities.

The design for the ET-LF filter cavity scheme is more complex than for ET-HF, and has to include a careful trade-off between excavation cost, expected optical losses and practical constraints for arranging the vacuum system.

C. Coupled Filter Cavities

The purpose of using filter cavities in the squeezing path is to replicate the quadrature rotation of the interferometer as seen by the signal light. For a detuned signal-recycled Michelson such as ET-LF, two separate rotations are required. Current plans for ET-LF achieve the desired rotation with two separate filter cavities in series, with each filter cavity producing a single rotation around its resonance. As a coupled cavity exhibits two separate resonances, these two independent filter cavities could potentially be replaced with a coupled filter cavity. To investigate this possibility, a model of a coupled filter cavity was numerically fit to give the same squeezing angle rotation as the two filter cavities, and then further optimised to maximise the quantum-noise limited sensitivity from 5–30 Hz.

Figure 11 compares the quantum-noise limited sensitivity of ET-LF for a 20 km coupled filter cavity vs 2×10 km filter cavities, both with and without losses. Optimal parameters are given in Table III. There are a few noteworthy points here. Firstly, from Figure 11, we can see that the fit was performed successfully, and as such a coupled filter cavity could in theory be used in place of two independent cavities in a detuned, dual-

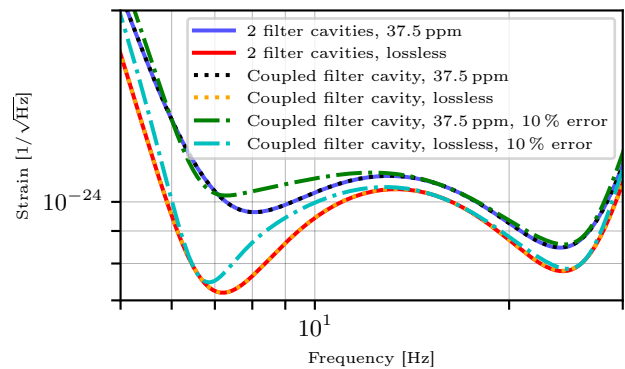


FIG. 11. Comparison of using two separate 10 km filter cavities vs. a coupled filter cavity totalling 20 km in ET-LF, both with lossless mirrors and 37.5 ppm loss per surface. The parameter with the lowest tolerance is the transmissivity of the middle mirror; the dash-dotted lines show the coupled cavity with a 10% increase in the middle mirror transmissivity from the optimal value, and the other parameters adjusted to compensate. A coupled filter cavity can be used to replicate the effects of two independent filter cavities in ET-LF. Perhaps surprisingly, the performance in the presence of losses is identical for the same loss per surface.

recycled Michelson such as ET-LF. Additionally, we see that the scaling of performance with mirror losses is identical in the coupled and independent cases. We also see that the performance of the filter cavity at low frequencies (~ 7 –12 Hz) is fairly sensitive to the middle mirror transmissivity.

There are a few motivating factors that make the coupled filter cavity design worth further study. When two individual cavities are used, some extra optics such as Faraday isolators must be introduced to direct the beam from one cavity to the next; this is not needed in a coupled filter cavity. Without these extra Faraday isolators the overall optical loss in the input squeezing path can be reduced [7], to increase the effective squeezing level achievable. Additionally, the same considerations for using a tuned vs. detuned Michelson for ET-LF from Section IIIB apply here: in the case of the coupled cavity scheme, the total filter cavity length is arranged sequentially in one long vacuum system, whereas the scheme with two filter cavities requires a shorter but wider space for two parallel vacuum systems. It should be noted that a coupled filter cavity of total length 10 km could provide much better sensitivity than a tuned detector in each of ET-LF's ‘dips’. This is shown explicitly in Figure 12.

In summary, a coupled filter cavity could be used in place of two independent filter cavities. There are two main advantages to this substitution: the lack of a need for an extra Faraday isolator results in lower losses in the squeezing path, and in the case of ET the form factor of the vacuum system could be advantageous. These advantages provide motivation for further study.

Type	Transmissivity		Tuning [degrees]	
Two cavities	$FC_{1,in} = 4.617 \times 10^{-3}$	$FC_{2,in} = 1.210 \times 10^{-3}$	$FC_{1,end} = 3.049 \times 10^{-1}$	$FC_{2,end} = -7.971 \times 10^{-2}$
Coupled cavity	$FC_{in} = 5.856 \times 10^{-3}$	$FC_{mid} = 3.099 \times 10^{-5}$	$FC_{mid} = 2.276 \times 10^{-1}$	$FC_{end} = 2.256 \times 10^{-1}$

TABLE III. Optimal filter cavity parameters for ET-LF, for both two filter cavities and a single coupled filter cavity. Each individual cavity is 10 km long, with 37.5 ppm loss per optic. Note the low transmissivity required for the middle mirror in the coupled filter cavity. As cavity length decreases, so too does the required value of middle mirror transmissivity.

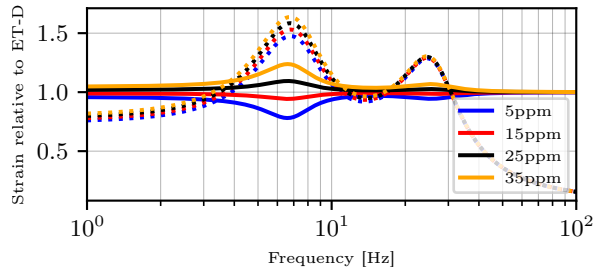


FIG. 12. Comparison of a detuned ET-LF with a 10 km total length coupled filter cavity (solid curves) and a tuned ET-LF with a single 10 km filter cavity (dotted curves). For all values of per-surface power loss plotted, the coupled filter cavity leads to better average sensitivity from ~ 4 –30 Hz, and a loss of 20 ppm brings the sensitivity in line with that of ET-D.

IV. SUMMARY

Practical considerations may motivate the introduction of longer signal recycling cavities in future detectors, such as ET. If the length of the SRC is not accounted for, it can lead to an overestimation of the sensitivity at high frequencies, as shown in Figure 2. This can be avoided by considering the SRC-arm system as a coupled cavity, the response of which is described loosely by a split resonance, with separation frequency ω_s and half-bandwidth γ_s , as given in Equation (2). We have shown that the change in the response of a detector due to a longer SRC can be counteracted by increasing both T_{itm} & T_{srn} . To maintain arm cavity power and thus sensitivity, we must also increase input power, either directly or by increasing the PRC gain. Increasing the length of the SRC, while maintaining sensitivity at high frequencies, therefore leads to an increase in the power incident on the central beamsplitter, as shown in Figure 5.

In the specific case of ET-HF, we suggest an SRC length of 100 m, which would result in a reduction of the quantum-noise limited sensitivity of only 25 % at 10 kHz compared to an SRC of negligible length. We further show how this loss of sensitivity can be compensated for, at the cost of increased laser power at the beamsplitter.

The scaling of this sensitivity with beamsplitter power can be seen in Figure 6. For ET-LF, the frequencies at which the decrease in sensitivity occurs are too high to be of consequence. Figure 7 shows that for a 100 m SRC, the reduction in sensitivity at 30 Hz is on the order of 0.1 %.

Constraints such as the size and cost of the underground infrastructure provide motivation for reducing the length of the filter cavities used for frequency-dependent squeezing in ET. This has the effect of increasing filter cavity loss per unit length, leading to a reduction in performance. For ET-HF, a much shorter filter cavity of, for example, 300 m has limited consequences, as thermal noise of the main interferometer remains the limiting factor in the frequency range affected by filter cavity losses. In ET-LF, the consequences of reducing the filter cavity lengths from 10 km to 1 km would be more severe, giving up to a factor of 2 reduction in quantum-noise limited sensitivity at 7 Hz for a currently achievable round-trip optical power loss of 40 ppm. However, with expected improvements in optical losses such as an increase in mirror surface quality, a significant reduction of the filter cavity length would be possible. In addition, the use of a coupled filter cavity in place of two independent filter cavities for ET-LF was investigated, and found to perform identically for the same length and per-surface loss. Combined with the fact that coupled cavities would use one less Faraday isolator in the injection path, which further reduces the optical losses, coupled filter cavities should be studied further.

ACKNOWLEDGMENTS

We are grateful to Jérôme Degallaix for providing information on optical losses and Jan Harms and Harald Lück for helpful comments. This work has been supported by the Science and Technology Facilities Council (STFC), A. Freise acknowledges support from a Royal Society Wolfson Fellowship which is jointly funded by the Royal Society and the Wolfson Foundation. This paper has the LIGO Document Number LIGO-P2000066.

[1] J. Aasi *et al.* (LIGO Scientific Collaboration), *Class. Quant. Grav.* **32**, 074001 (2015), arXiv:1411.4547 [gr-qc].

[2] F. Acernese *et al.* (Virgo Collaboration), *Class. Quant. Grav.* **32**, 024001 (2015), arXiv:1408.3978 [gr-qc].

- [3] M. Punturo *et al.*, Classical and Quantum Gravity **27**, 084007 (2010).
- [4] S. Hild *et al.*, Classical and Quantum Gravity **28**, 094013 (2011).
- [5] The ET Science Team, *Einstein gravitational wave Telescope conceptual design* (European Commission, 2011).
- [6] H. Grote, K. Danzmann, K. L. Dooley, R. Schnabel, J. Slutsky, and H. Vahlbruch, Phys. Rev. Lett. **110**, 181101 (2013).
- [7] M. Tse *et al.*, Phys. Rev. Lett. **123**, 231107 (2019).
- [8] F. Acernese *et al.*, Phys. Rev. Lett. **123**, 231108 (2019).
- [9] H. J. Kimble, Y. Levin, A. B. Matsko, K. S. Thorne, and S. P. Vyatchanin, Phys. Rev. D **65**, 022002 (2001).
- [10] S. Hild, S. Chelkowski, A. Freise, J. Franc, N. Morgado, R. Flaminio, and R. DeSalvo, Class. Quant. Grav. **27**, 015003 (2010), arXiv:0906.2655 [gr-qc].
- [11] J. Mizuno, *Comparison of optical configurations for laser-interferometric gravitational-wave detectors*, Ph.D. thesis, Hannover U. (1995).
- [12] M. Evans, L. Barsotti, P. Kwee, J. Harms, and H. Miao, Phys. Rev. D **88**, 022002 (2013).
- [13] Y. Levin, Phys. Rev. D **57**, 659 (1998).
- [14] A. Freise, FINESSE: frequency domain interferometer simulation software (2020), <http://www.gwoptics.org/finesse>.
- [15] A. Freise, G. Heinzel, H. Lck, R. Schilling, B. Willke, and K. Danzmann, Classical and Quantum Gravity **21**, S1067S1074 (2004).
- [16] A. C. Green, D. D. Brown, M. Dovale-Álvarez, C. Collins, H. Miao, C. M. Mow-Lowry, and A. Freise, Classical and Quantum Gravity **34**, 205004 (2017).
- [17] A. Buonanno and Y.-b. Chen, Phys. Rev. **D67**, 062002 (2003), arXiv:gr-qc/0208048 [gr-qc].
- [18] A. Thüring, H. Lück, and K. Danzmann, Phys. Rev. E **72**, 066615 (2005).
- [19] D. Martynov *et al.*, Phys. Rev. (2019), arXiv:1901.03885 [astro-ph.IM].
- [20] T. Isogai, J. Miller, P. Kwee, L. Barsotti, and M. Evans, Opt. Express **21**, 30114 (2013), arXiv:1310.1820 [physics.optics].
- [21] P. Kwee, J. Miller, T. Isogai, L. Barsotti, and M. Evans, Phys. Rev. **D90**, 062006 (2014), arXiv:1704.03531 [physics.optics].
- [22] P. Purdue and Y. Chen, Phys. Rev. **D66**, 122004 (2002), arXiv:gr-qc/0208049 [gr-qc].
- [23] J. Degallaix, C. Michel, B. Sassolas, A. Allocca, G. Cagnoli, L. Balzarini, V. Dolique, R. Flaminio, D. Forest, M. Granata, B. Lagrange, N. Straniero, J. Teillon, and L. Pinard, J. Opt. Soc. Am. A **36**, C85 (2019).